Room-Temperature Quantitative Quantum Sensing of Lithium Ions with a Radical-Embedded Metal–Organic Framework

Lei Sun,[1,†,‡,*] Luming Yang,[2,†] Jin-Hu Dou,[2] Jian Li[3], Grigorii Skorupskii,[2] Michael Mardini,[2,4] Kong Ooi Tan,[2,4,¶] Tianyang Chen,[2] Chenyue Sun,[2] Julius J. Oppenheim,[2] Robert G. Griffin,[2,4] Mircea Dincă,[2,*] Tijana Rajh[1,5,*]

[1]Center for Nanoscale Materials, Argonne National Laboratory, Lemont, Illinois 60439, USA

[2]Department of Chemistry, Massachusetts Institute of Technology, Cambridge, Massachusetts 02139, USA

[3]Department of Fibre and Polymer Technology, KTH Royal Institute of Technology, Teknikringen 56, Stockholm 10044, Sweden

[4]Francis Bitter Magnet Laboratory, Massachusetts Institute of Technology, Cambridge, Massachusetts 02139, USA

[5]The School for Molecular Sciences, Arizona State University, Tempe, Arizona 85281, USA

ABSTRACT: Recent advancements in quantum sensing have sparked transformative detection technologies with high sensitivity, precision, and spatial resolution. Owing to their atomic-level tunability, molecular qubits and ensembles thereof are promising candidates for sensing chemical analytes. Here, we show quantum sensing of lithium ions in solution at room temperature with an ensemble of organic radicals integrated in a microporous metal–organic framework (MOF). The organic radicals exhibit electron spin coherence and microwave addressability at room temperature, thus behaving as qubits. The high surface area of the MOF promotes accessibility of the guest analytes to the organic qubits, enabling unambiguous identification of lithium ions and quantitative measurement of their concentration through relaxometric and hyperfine spectroscopic methods based on electron paramagnetic resonance (EPR) spectroscopy. The sensing principle presented in this work is applicable to other metal ions with nonzero nuclear spin.

INTRODUCTION

Quantum sensing exploits quantum phenomena to measure physical quantities including magnetic field, electric field, temperature, pressure, pH, time, and frequency, among others.[1] The ability to coherently address single qubits and qubit ensembles has sparked revolutionary sensing technologies with nanoscale spatial resolution as well as ultrahigh sensitivity and precision,[1] enabling atomic-level magnetic resonance imaging,[2] single-molecule magnetometry,[3,4] and magnetic imaging of living cells.[5]

Despite these advances and applications, an outstanding open challenge is to apply quantum sensing for quantifying chemical analytes in ambient conditions, which could be instrumental for a range of technologies spanning biological systems and energy storage devices.[6–8] The vast majority of qubits, including superconducting circuits,[9] semiconductor quantum dots,[10] trapped ions,[11] and neutral atoms,[12] have limited application in ambient conditions because they typically require cryogenic temperature and/or strictly controlled environments. Although qubits based on solid-state defects such as nitrogen–vacancy (NV) centers in diamond can operate at room temperature and have been used to detect chemical analytes through T_1 relaxometry[13] and magnetic resonance spectroscopy,[3,4,14] they are typically buried inside the insulating solid, preventing close contact and strong interaction with chemicals.[4,6] Furthermore, solid-state defect qubits most often lack designability and tunability that are critical for selective and simultaneous sensing of multiple species.[6] To this end, molecular qubits, a class of paramagnetic molecules that exhibit electron spin coherence,[15] are promising alternative candidates that can be modified with selective and strong binding sites for chemical analytes[16] and, in certain cases, can operate at room temperature.[17–22] Integrating solid-state materials with molecular qubits can therefore create a powerful new platform for quantum sensing.

Recent research on molecular qubits based on transition-metal or lanthanide electron spin centers[15,23–25] has revealed design rules for achieving millisecond phase memory time[26,27] or optical addressability[28] at cryogenic temperature, and has established strategies to construct spatially ordered molecular qubit arrays.[29,30] Nonetheless, except for a small number of examples with Cu(II), V(IV), or Y(II) as spin centers,[17–22] most metal-based molecular qubits do not operate at room temperature due to fast spin–lattice relaxation induced by spin-orbit couplings at the metal sites.[20,31,32] In this regard, organic radicals with unpaired electron spins residing on light atoms with negligible spin-orbit coupling, such as carbon, nitrogen, and oxygen, are promising alternatives. When dilute, these can maintain spin coherence at room temperature with microsecond-scale phase memory time.[31,33] Although these properties have enabled wide use of organic radicals as spin labels in biological systems[34] and as polarizing agents

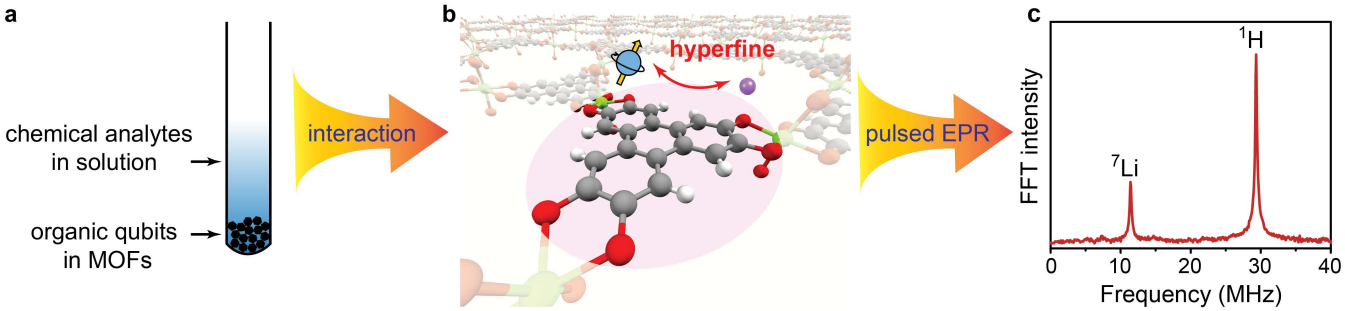

Figure 1. Room-temperature quantum sensing using organic radicals in MOFs. (a) MOF particles with organic qubits are suspended in a solution containing the desired analyte, in this case a solution of $LiClO_4$ in THF. (b) The chemical analytes are adsorbed into the MOF and interact with the embedded radicals through hyperfine coupling. (c) Nuclei interacting with the radical qubit can be identified based on the hyperfine spectrum, which further allows quantification of the chemical analytes.

in dynamic nuclear polarization,[35] organic radicals remain unexplored for quantum sensing.

One powerful approach for achieving room-temperature quantitative sensing of chemical analytes is relaxometry, which probes spin relaxation to relay information about concentration.[36] Although widely used in magnetic resonance imaging and recently demonstrated for quantum sensors based on NV centers in diamond,[13] this technique still has limited application in chemical identification and simultaneous sensing of multiple analytes. A related, but potentially more versatile approach is the detection of nuclear hyperfine fields stemming from the coupling between an electron spin qubit and nuclear spins in its environment. This can be achieved by hyperfine spectroscopy, which can identify the nuclear species and possibly characterize coupling strengths (Figure 1c).[37] Because hyperfine fields are typically limited to short distances, close contact between the electron spin qubit and the target nuclei is a key requirement for implementing this sensing scheme.[6]

Thanks to their high surface area, MOFs are ideal hosts for molecular qubits to promote qubit–analyte accessibility. MOFs are porous ordered solids composed of inorganic and organic molecular building blocks.[38] They typically contain nanoscale or sub-nanoscale pores that have enabled their use in traditional sensing applications.[39,40] Previously, it has been shown that electron spins in microporous zeolites and MOFs can be used to detect guest species by hyperfine spectroscopy, but these demonstrations were performed at cryogenic temperatures (below 10 K) due to the limitation of electron spin coherence and/or sensitivity.[41–43] Here, we seek to incorporate organic radicals into the MOF backbone to enable room-temperature operability while preserving pore accessibility, leading to close radical–analyte contacts through adsorption (Figure 1b). In addition, MOFs can be elaborated as inert and insoluble solids for either liquid or solution phase analytes (Figure 1a). This suppresses radical tumbling typical for liquids,[31] and improves detection sensitivity by concentrating the solid-embedded radicals to an extent that is unreachable with soluble species.

A material that showcases these concepts is $\{[Mg(H_2O)_2]_3HOTP_2\}\{[Mg(H_2O)_4]_3HOTP\}_2$ (MgHOTP, HOTP = 2,3,6,7,10,11-hexaoxytriphenylene), a new MOF bearing closed-shell metal ions, nanoscale pores, and organic radicals as the only paramagnetic centers (Figure 1). Besides avoiding electron–electron relaxation pathways, diamagnetic Mg^{2+} ions are ideal for this application because the high natural abundance of ^{24}Mg (90%), an isotope with zero nuclear spin, also minimizes electron–nucleus relaxation. The tritopic ligand 2,3,6,7,10,11-hexahydroxytriphenylene (HHTP) is a common building block in two-dimensional (2D) porous MOFs,[44] whose spontaneous oxidation generates a radical.[45,46] Using EPR spectroscopy, we demonstrate that the radicals in MgHOTP behave as electron spin qubits, whose quantum states can be partially polarized by an external magnetic field, manipulated by microwave pulses, and read out through electron spin echo schemes. We further demonstrate quantitative detection of lithium ions (Li^+) in solution at room temperature using MgHOTP qubits with relaxometry and hyperfine spectroscopy.

RESULTS AND DISCUSSION

Synthesis and structure of MgHOTP. A solvothermal aerobic reaction between magnesium acetate and HHTP in a mixture of water and dimethyl sulfoxide yields MgHOTP as a navy-black microcrystalline powder composed of hexagonal rod-like single crystals, with the longest dimension ranging from 0.5 μm to 13 μm (Figures S1–S3). The single-crystal structure of MgHOTP was solved through a combined refinement of continuous rotation electron diffraction (cRED) and synchrotron powder X-ray diffraction (PXRD) data (Figures S4–S7, Table S1).[47,48] It consists of two components: extended 2D honeycomb sheets with the formula of $[Mg(H_2O)_2]_3HOTP_2$ (Figure 2a, c) and isolated molecular clusters with the formula of $[Mg(H_2O)_4]_3HOTP$ (Figure 2b, d; see discussion about charge assignment in the Supporting Information). The molecular clusters sit in-between neighboring sheets and manifest alternating interlayer spacing of 3.2 Å and 3.5 Å (Figure 2e); HOTP ligands in the clusters and those within the sheets are eclipsed with a rotation (Figure 2b). Cryogenic electron microscopy (cryo-EM) and fast Fourier transform (FFT) analysis of MgHOTP corroborate the structure obtained by cRED and PXRD (Figure 2f–h). The eclipsed stacking in MgHOTP leads to one-dimensional (1D) pores with a diameter of approximately 1.4 nm (Figure 2a, b). The desolvated framework exhibits a Brunauer–Emmet–Teller surface area of 481 m^2/g, as determined by N_2 adsorption at 77 K (Figure S8–S9). Critically, these pores provide sufficiently large apertures for solvated metal ions to enter and interact with the HOTP radicals.

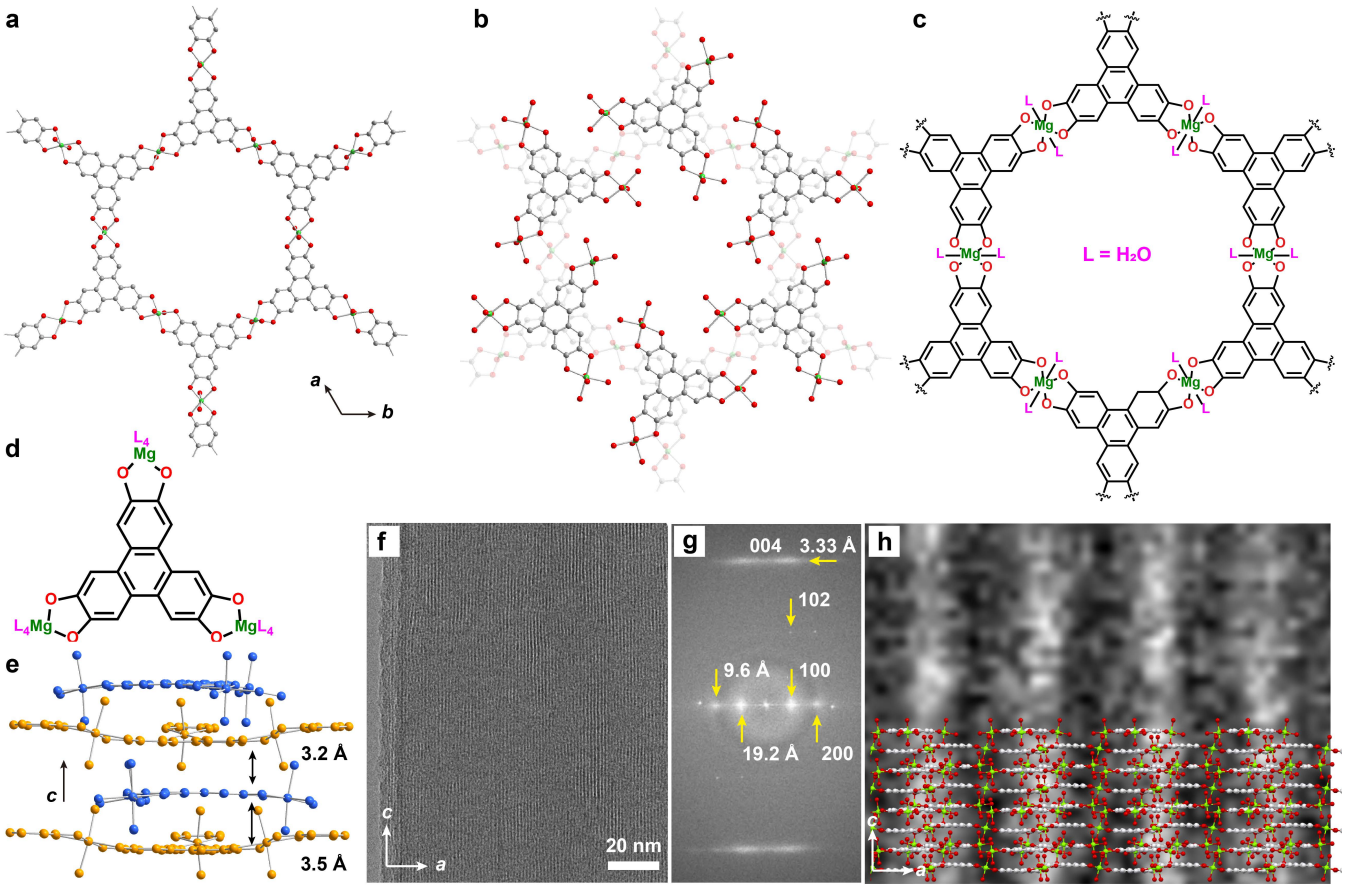

Figure 2. Single-crystal structure of MgHOTP derived from cRED and synchrotron PXRD. (a, b) Structural representation of single and double layers of MgHOTP viewed down the crystallographic *c* axis, with (b) depicting the rotated eclipsed stacking between the clusters and the sheets. Green, red, and gray spheres represent Mg, O, and C atoms, respectively. H atoms are omitted for clarity. (c, d) Chemical structures of a portion of the $[Mg(H_2O)_2]_3HOTP_2$ sheet and one $[Mg(H_2O)_4]_3HOTP$ cluster, respectively. (e) View parallel to the crystallographic *ab* plane, showing the deviation from planarity in the sheets (yellow) and the clusters (blue), as well as the two distinct interplanar distances. (f) Cryo-EM image of MgHOTP. (g) FFT of (f). (h) High-magnification micrograph from (f), with visible lattice fringes. High-contrast fringes perpendicular to the pore walls are spaced at 19.2 Å. They are overlayed with a structural model of MgHOTP showing the fringes that match well with the d-spacing along the crystallographic *a* axis.

Organic electron spin qubits in MgHOTP. To probe the HOTP-centered organic radicals, we performed continuous-wave (CW) and pulsed EPR measurements on MgHOTP crystallites at room temperature (296 K). The X-band (9–10 GHz) CW EPR spectrum displays a single resonance peak at g = 2.00373 with a linewidth of 0.33 mT (Figure 3a). The D-band (140 GHz) echo-detected field sweep (EDFS) gave g-anisotropy values $g_{\parallel}$ = 2.00221 and $g_{\perp}$ = 2.00497 (Figure S10). These g values are typical for phenoxyl radicals.[45] Quantitative CW EPR analysis revealed that 1–2% of HOTP ligands contain a radical (Figures S11, Table S2–S3), corresponding to an electron spin concentration between 2 × 10^{-2} mol/L and 4 × 10^{-2} mol/L. Note that saturated solutions of the free-ligand HHTP in typical organic solvents such as tetrahydrofuran (THF) do not show observable CW or pulsed EPR signals. The relatively high radical concentration on HOTP is thus available only by integrating this ligand within the MOF.

Pulsed EPR characterization provided key evidence in testing qubit-type behavior of HOTP radicals. Appropriate microwave pulses can orient electron spin qubits on arbitrary positions, contrasting with electron spin bits used in regular spintronic devices, which exclusively use binary positions for information processing.[23,24] When electron spins behave like qubits, under magnetic field, they satisfy the Rabi relationship $\hbar\omega_{\mathrm{Rabi}} = g\mu_B SB_1$, where $\hbar$ is the reduced Planck constant, ω_{Rabi} is the Rabi frequency, μ_B is the Bohr magneton, and B_1 is the microwave magnetic field. Importantly, under microwave pulses of various power and length, MgHOTP exhibits oscillations of spin orientations with frequencies ω_{Rabi} that are linearly dependent on B_1 (Figure 3b, Figure S12), providing key evidence that radicals in MgHOTP are suitable for single-qubit quantum gate operations.[24] More practically, an electron spin qubit must also possess long spin–lattice relaxation time (T_1) and phase memory time (T_m) to ensure sufficient duration of its polarization and coherence.[31,49] To measure T_1 and T_m, we employed inversion recovery and Hahn echo decay pulse sequences, respectively, on dry powders of MgHOTP. Depending on the synthetic conditions of each batch of MgHOTP, these measurements gave room-temperature values of T_1 ranging from 9.48 μs to 21.34 μs and T_m ranging from 153 ns to 239 ns at 296 K (Figure 3c, d, Figure S13), qualifying MgHOTP as a potential candidate for quantum sensing of chemical analytes under ambient conditions.

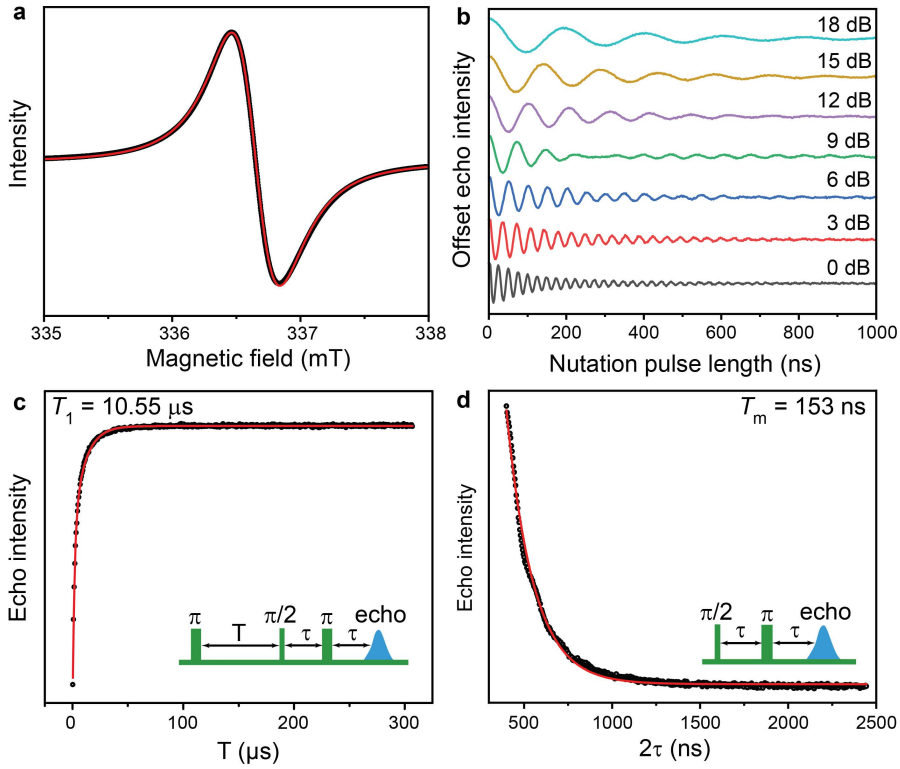

Figure 3. Organic electron spin qubits in dry powders of MgHOTP at room temperature. (a) CW EPR spectrum. The red line is the fitting curve obtained from Dysonian line shape using S = ½ and g = 2.00373. (b) Nutation experiments at various microwave attenuations. (c) Inversion recovery measurement of T_1. The red line is a bi-exponential decay fitting curve. Inset: pulse sequence for the inversion recovery experiment. (d) Hahn echo decay measurement of T_m. The red line is a mono-exponential decay fitting curve. Inset: pulse sequence for the Hahn echo decay experiment. These data were collected with X-band EPR at 296 K.

Quantitative quantum sensing of lithium ions by MgHOTP. To demonstrate the utility of MgHOTP in quantum sensing, we targeted the detection of Li^+ ions because of their important role in energy-related and biological applications.[8] Additionally, Li^+ should show affinity towards the oxygen atoms lining the pores of MgHOTP,[50] and the major Li isotope, ^{7}Li (92.4% natural abundance), has a unique nuclear Larmor frequency, which minimizes potential interference from other nuclei. Treatment of MgHOTP powders with solutions of $LiClO_4$ in THF leads to incorporation of Li^+ within the MOF without significantly affecting the *g*-factor of the organic radical or its qubit behavior (Figures S12, S14, Table S4). However, T_1 and T_m changed when the concentration of Li^+ ([Li^+]) ranged between 0.1 mol/L and 2.0 mol/L, giving rise to relaxometric detection in this range. For instance, in a given MgHOTP batch whose dry powder exhibits T_1 = 10.55 μs and T_m = 153 ns (Figure 3c, d), when [Li^+] < 0.1 mol/L, both T_1 and T_m remain relatively constant (T_1 = 20 ~ 21 μs, T_m = 190 ~ 200 ns), but increasing [Li^+] reduces both T_1 and T_m significantly, reaching T_1 = 12.55 μs and T_m = 169 ns for [Li^+] = 2 mol/L (Figure 4a, Figure S15, Table S5), likely a result of radical–Li^+ hyperfine interaction. Indeed, ^{6}Li solid-state nuclear magnetic resonance (NMR) spectroscopic studies confirmed a significant reduction of the nuclear T_1 of $^6Li^+$ upon incorporation into MgHOTP (Figures S16–S17).

Interrogating the radical–Li^+ hyperfine interaction can provide much higher sensitivity for Li^+ sensing. This interaction can be probed by combination-peak electron spin echo envelope modulation (CP-ESEEM) spectroscopy,[37,51] which balances sensitivity, resolution, and acquisition time (Figure S18) by employing a 4–pulse sequence (π/2 – τ – π/2 – T – π – T – π/2 – τ – echo), with the nuclear spin precession modulating electron spin echo decay during evolution times T (Figure 4b). In the weak-coupling regime, where the hyperfine constant is much smaller than the nuclear Larmor frequency (ω_I), as is the case for MgHOTP radical–^{7}Li and radical–^{1}H hyperfine interactions revealed by hyperfine sublevel correlation (HYSCORE) spectroscopic studies (Figure S19–S20), the frequency-domain CP-ESEEM spectrum displays peaks at $2\omega_I$ of the hyperfine nuclei.[37] Therefore, CP-ESEEM can serve as a decisive technique for the detection of various elements, ^{7}Li and ^{1}H in this case, that bear distinguishing Larmor frequencies.

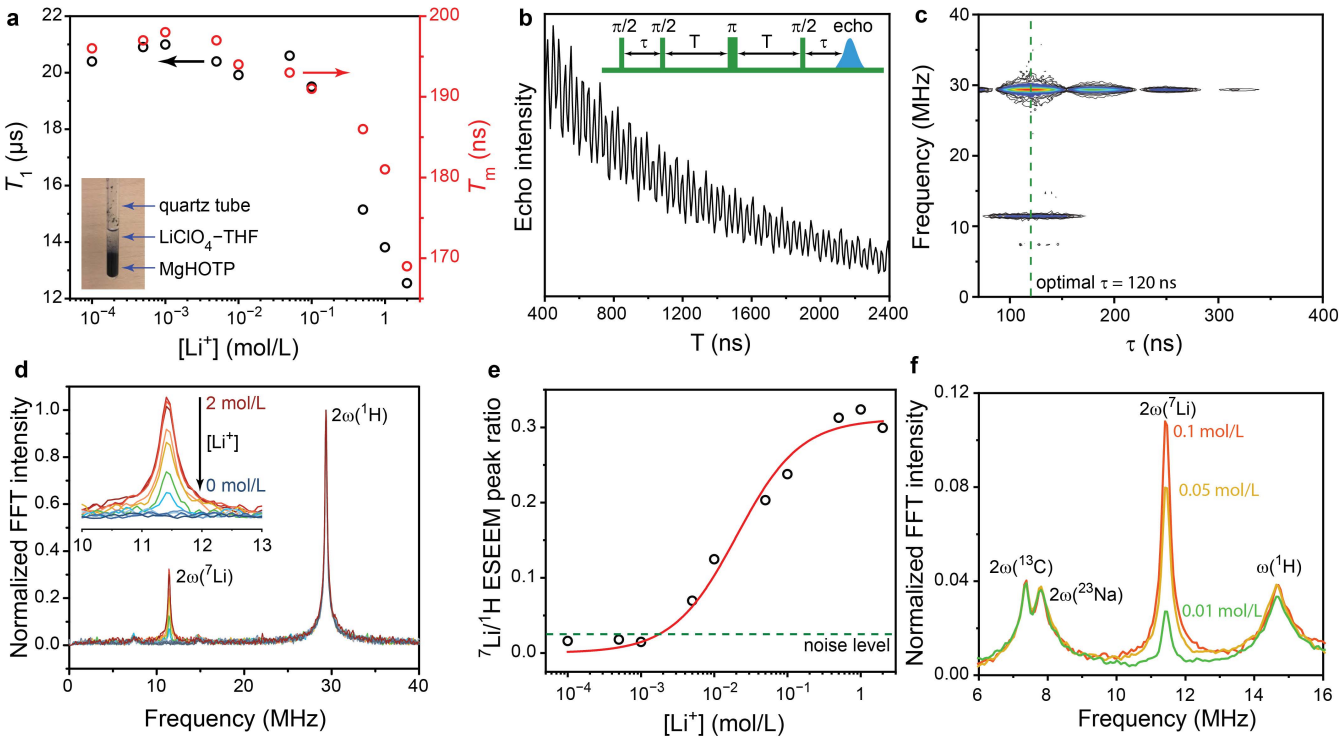

Figure 4. Quantitative sensing of Li^+ in THF solution by MgHOTP at room temperature. (a) T_1 and T_m of MgHOTP in THF solutions of $LiClO_4$ with various [Li^+]. Inset: picture of a sample for the EPR measurement. (b) Portion of a time-domain CP-ESEEM spectrum of MgHOTP in a THF solution of $LiClO_4$ where [Li^+] = 2.0 mol/L. This measurement takes approximately 40 minutes to gain high signal-to-noise ratio. Inset: pulse sequence of CP-ESEEM. (c) 2D spectrum of CP-ESEEM collected with various τ values. (d) Frequency-domain CP-ESEEM spectra of MgHOTP in THF solutions of $LiClO_4$ with various [Li^+]. The spectra were normalized to the 2ω(^{1}H) peaks. Inset: zoom-in view on the 2ω(^{7}Li) peaks. (e) Relationship between 2ω(^{7}Li)/ 2ω(^{1}H) ESEEM peak ratio and [Li^+]. The former was calculated by dividing the maximum of the 2ω(^{7}Li) peak with the maximum of the 2ω(^{1}H) peak in each spectrum. Red curve represents fit of the data to Langmuir adsorption model. Green dashed line represents the noise level estimated based on the spectrum of MgHOTP in pure THF. (f) Frequency-domain CP-ESEEM spectra of MgHOTP in THF solutions with 0.1 mol/L $NaClO_4$ and various concentrations of $LiClO_4$. The spectra were normalized to the 2ω(^{1}H) peaks, which is not shown for clarity.

The X-band CP-ESEEM spectrum of MgHOTP soaked in a THF solution with [Li^+] = 2 mol/L displays two peaks at 11.41 MHz and 29.34 MHz under a field of 344.53 mT, corresponding to $2\omega_I$ of ^{7}Li and ^{1}H, respectively (Figure 4d). These peaks reflect the modulation of the HOTP electron spin by the nuclear spins of ^{7}Li and ^{1}H in the sub-nanometer proximity. They decisively identify ^{7}Li and ^{1}H in the environment surrounding HOTP. The ^{1}H peak relates to MOF components or guest solvent molecules, as also confirmed by control CP-ESEEM studies of MgHOTP in deuterated solvents (Figures S21–S23). In contrast, the ^{7}Li peak unambiguously confirms that MgHOTP behaves as a quantum sensor for Li^+ at room temperature. The absence of ^{35}Cl and ^{37}Cl signals in CP-ESEEM spectra suggests negligible interaction between the MgHOTP qubits and ClO_4^-, likely due to Coulombic repulsion between the anions and the oxygen-rich pore surface of the framework. Indeed, CP-ESEEM signals from anions are also absent when employing other Li^+ salts such as LiCl and LiBr (Figure S24), demonstrating the selectivity of MgHOTP towards cations.

Notably, CP-ESEEM with MgHOTP enables quantitative detection of even small concentrations of Li^+, because the ESEEM signal from ^{7}Li can be referenced to that of an internal standard, here ^{1}H (see theoretical analysis in Supporting Information).[52,53] We took advantage of the narrow linewidth of MgHOTP (Figure 3a, Figure S25)[49] and adopted an optimal CP-ESEEM delay time τ = 120 ns, which gives maximum modulation depth from ^{7}Li (Figure 4c, Figures S26–S28). With these parameters, all CP-ESEEM measurements display ^{1}H peaks with the same line shape for any [Li^+] in the range 1×10^{-4} mol/L to 2 mol/L (Figure 4d), showing minimal influence of ^{7}Li nuclear spins on the radical–^{1}H interactions. For [Li^+] ≥ 5×10^{-3} mol/L, the relative peak intensity of ^{7}Li increases sigmoidally with log[Li^+], approaching a plateau above 0.5 mol/L (Figure 4e, Figures S29–S30, Table S6–S8). This relationship fits well to the Langmuir adsorption model, which describes monolayer physical adsorption on a surface.[54] It suggests that sensing with MgHOTP is reserved to Li^+ ions proximal to the pore surface, as would be expected given the fast decay of the radical–^{7}Li hyperfine interaction with distance. Interestingly, the Langmuir behavior provides thermodynamic data that calibrate the strength of Li^+ adsorption onto MgHOTP: fitting the data to the Langmuir model gives an adsorption equilibrium constant of 49.5 ± 10.2 L/mol, consistent with a weak Li^+–MOF interaction.[55] Altogether, these results demonstrate that using CP-ESEEM with MgHOTP enables quantitative sensing of Li^+ ions in the range of 5×10^{-3} mol/L – 0.5 mol/L under ambient conditions, two-order of magnitude improvement over relaxometry. CP-ESEEM and relaxometry are nevertheless complimentary: their combination enables an effective quan-

tum sensing range of 5×10^{-3} mol/L – 2 mol/L.

Crucially, the principles and methods above can be extended for the detection of other metal ions with nonzero nuclear spin and, by extension, should allow simultaneous detection of multiple metal ions that display distinguishable Larmor frequencies. We demonstrated this concept by a sample of MgHOTP soaked in a THF solution of 0.1 mol/L $LiClO_4$ and 0.1 mol/L $NaClO_4$. A CP-ESEEM spectrum of this sample at 296 K under a field of 344.64 mT revealed a peak at 7.81 MHz, the expected $2\omega_I$ value for ^{23}Na, in addition to peaks corresponding to ^{1}H, ^{7}Li, and ^{13}C (Figure 4f). The ^{23}Na peak is significantly weaker than the ^{7}Li peak, indicating weaker interaction between the framework and Na^+. With the $2\omega_I$ of ^{1}H peak as an internal reference, decreasing the $[Li^+]$ to 0.05 mol/L and 0.01 mol/L while maintaining a constant $[Na^+]$ caused concomitant decrease in the intensity of the ^{7}Li peak without distinguishable changes in the ^{23}Na peak (Figure 4f, Figure S31, Table S9). These experiments demonstrate that MgHOTP is capable of simultaneous detection of Li^+ and Na^+ as well as quantification of Li^+ in the presence of Na^+. Because sensitivity is a proxy for the binding strength of metal ions to MgHOTP, it is reasonable to expect that quantum sensing of divalent and multivalent metal ions would be even more efficient. Applying this methodology to multivalent ions and particular combinations of ions relevant for different technologies are obvious future extensions for this work.

CONCLUSIONS AND OUTLOOK

The foregoing results convey the first demonstration of room-temperature quantum sensing using a MOF containing organic qubits. Relaxometry and CP-ESEEM combine to provide a wide range (5×10^{-3} mol/L – 2 mol/L) of sensitivity for Li^+ ions, as well as direct quantification of mixed ion solutions. Although this Li^+ detection threshold is still not comparable with those of optical or electrochemical sensing strategies,[8,56] it is sufficient for quantitative detection in battery applications[7]. The sensitivity could be improved with high-frequency/high-field EPRs and by employing hyperfine spectroscopic methods based on dynamical decoupling[57], which may as well assist studies of MOF–guest binding structures because these techniques reveal more detailed hyperfine spectra.

The quantum sensing methodology derived in this work suggest several clear directions that could offer additional breadth and utility. Functionalization of the MOF with specific metal-binding groups should further enhance selectivity for those ions.[16] Adapting this methodology to lower-frequency EPR measurements, where the microwave permittivity of strongly polar solvents is much higher,[58] should further broaden the utility of this quantum sensing protocol to biological and battery-related applications. Finally, the quantum sensing principles demonstrated herein are transferrable to other pulsed EPR techniques. Ultimately, single ion/molecule sensitivity may be achieved by addressing single molecular electron spin qubits with optically or electrically detected magnetic resonance.[28,59]

ASSOCIATED CONTENT

Supporting Information

The Supporting Information is free of charge on the ACS Publication website.

Full descriptions of experimental methods, electron diffraction micrographs, PXRD patterns, thermogravimetric analysis, N_2 adsorption isotherm, quantitative EPR analysis, solid-state nuclear magnetic resonance spectroscopic studies, pulsed EPR characterization results, and theoretical analysis for quantitative sensing by CP-ESEEM (PDF)

Accession Codes

The crystallographic information has been deposited in the Cambridge Crystallographic Data Center (CCDC) under accession code 2103823.

AUTHOR INFORMATION

Corresponding Authors

* Lei Sun – Email: sunlei@westlake.edu.cn

Mircea Dincă – Email: mdinca@mit.edu

Tijana Rajh – Email: tijana.rajh@asu.edu

Present Addresses

‡ School of Science, Westlake University and Westlake Institute for Advanced Study, 18 Shilongshan Road, Hangzhou, Zhejiang 310024, China

¶ Laboratoire des Biomolécules, LBM, Département de Chimie, École Normale Supérieure, PSL University, Sorbonne Université, CNRS, 75005 Paris, France

Author Contributions

†L. S. and L. Y. contributed equally.

Notes

The authors declare no competing financial interest.

ACKNOWLEDGMENT

This work was performed, in part, at the Center for Nanoscale Materials and used resources of Advanced Photon Source, both DOE Office of Science User Facilities, and was supported by Laboratory Directed Research and Development (LDRD) funding from Argonne National Laboratory, provided by the Director, Office of Science, of the U.S. Department of Energy under Contract No. DE-AC02-06CH11357. Work in the Dincă lab was supported by the Army Research Office (Award W911NF-21-1-0124). The cRED/MicroED data was collected at the Electron Microscopy Center (EMC), Department of Materials and Environmental Chemistry (MMK) in Stockholm University with the support of the Knut and Alice Wallenberg Foundation (KAW, 2012-0112) through the 3DEM-NATUR project. Work in the Griffin lab was supported by the National Institute of General Medical Sciences (GM132997 and GM132079). We thank Dr. Walter Massefski for assistance in solid-state NMR measurements and thank Dr. Jenna L. Mancuso and Dr. Christopher H. Hendon for helpful discussion.

REFERENCES

(1) Degen, C. L.; Reinhard, F.; Cappellaro, P. Quantum sensing. *Rev. Mod. Phys.* **2017**, *89*, 035002.

(2) Abobeih, M. H.; Randall, J.; Bradley, C. E.; Bartling, H. P.; Bakker, M. A.; Degen, M. J.; Markham, M.; Twitchen, D. J.; Taminiau, T. H. Atomic-scale imaging of a 27-nuclear-spin cluster using a quantum sensor. *Nature* **2019**, *576*, 411–415.

(3) Shi, F.; Zhang, Q.; Wang, P.; Sun, H.; Wang, J.; Rong, X.; Chen, M.; Ju, C.; Reinhard, F.; Chen, H.; Wrachtrup, J.; Wang, J.; Du, J. Single-protein spin resonance spectroscopy under ambient conditions. *Science* **2015**, *347*, 1135–1138.

(4) Lovchinsky, I.; Sushkov, A. O.; Urbach, E.; de Leon, N. P.; Choi, S.; De Greve, K.; Evans, R.; Gertner, R.; Bersin, E.; Müller, C.; McGuinness, L.; Jelezko, F.; Walsworth, R. L.; Park, H.; Lukin, M. D. Nuclear magnetic resonance detection and spectroscopy of single proteins using quantum logic. *Science* **2016**, *351*, 836–841.

(5) Le Sage, D.; Arai, K.; Glenn, D. R.; DeVience, S. J.; Pham, L. M.; Rahn-Lee, L.; Lukin, M. D.; Yacoby, A.; Komeili, A.; Walsworth, R. L. Optical magnetic imaging of living cells. *Nature* **2013**, *496*, 486–489.

(6) Yu, C.-J.; von Kugelgen, S.; Laorenza, D. W.; Freedman, D. E. A molecular approach to quantum sensing. *ACS Cent. Sci.* **2021**, *7*, 712–723.

(7) Dutoit, C.-E.; Tang, M.; Gourier, D.; Tarascon, J.-M.; Vezin, H.; Salager, E. Monitoring metallic sub-micrometric lithium structures in Li-ion batteries by in situ electron paramagnetic resonance correlated spectroscopy and imaging. *Nat. Commun.* **2021**, *12*, 1410.

(8) Villemin, E.; Raccurt, O. Optical lithium sensors. *Coord. Chem. Rev.* **2021**, *435*, 213801.

(9) Blais, A.; Grimsmo, A. L.; Girvin, S. M.; Wallraff, A. Circuit quantum electrodynamics. *Rev. Mod. Phys.* **2021**, *93*, 025005.

(10) Kloeffel, C.; Loss, D. Prospects for spin-based quantum computing in quantum dots. *Annu. Rev. Condens. Matter Phys.* **2013**, *4*, 51–81.

(11) Bruzewicz, C. D.; Chiaverini, J.; McConnell, R.; Sage, J. M. Trapped-ion quantum computing: progress and challenges. *Appl. Phys. Rev.* **2019**, *6*, 021314.

(12) Saffman, M. Quantum computing with atomic qubits and Rydberg interactions: progress and challenges. *J. Phys. B: At. Mol. Opt. Phys.* **2016**, *49*, 202001.

(13) Sushkov, A. O.; Chisholm, N.; Lovchinsky, I.; Kubo, M.; Lo, P. K.; Bennett, S. D.; Hunger, D.; Akimov, A.; Walsworth, R. L.; Park, H.; Lukin, M. D. All-optical sensing of a single-molecule electron spin. *Nano Lett.* **2014**, *14*, 6443–6448.

(14) Miller, B. S.; Bezinge, L.; Gliddon, H. D.; Huang, D.; Dold, G.; Gray, E. R.; Heaney, J.; Dobson, P. J.; Nastouli, E.; Morton, J. J. L.; McKendry, R. A. Spin-Enhanced Nanodiamond Biosensing for Ultrasensitive Diagnostics. *Nature* **2020**, *587*, 588–593.

(15) Wasielewski, M. R.; Forbes, M. D. E.; Frank, N. L.; Kowalski, K.; Scholes, G. D.; Yuen-Zhou, J.; Baldo, M. A.; Freedman, D. E.; Goldsmith, R. H.; Goodson III, T.; Kirk, M. L.; McCusker, J. K.; Ogilvie, J. P.; Shultz, D. A.; Stoll, S.; Whaley, K. B. Exploiting chemistry and molecular systems for quantum information science. *Nat. Rev. Chem.* **2020**, *4*, 490–504.

(16) Yeung, M. C.-L.; Yam, V. W.-W. Luminescent cation sensors: from host–guest chemistry, supramolecular chemistry to reaction-based mechanisms. *Chem. Soc. Rev.* **2015**, *44*, 4192–4202.

(17) Bader, K.; Dengler, D.; Lenz, S.; Endeward, B.; Jiang, S.-D.; Neugebauer, P.; van Slageren, J. Room temperature quantum coherence in a potential molecular qubit. *Nat. Commun.* **2014**, *5*, 5304.

(18) Atzori, M.; Tesi, L.; Morra, E.; Chiesa, M.; Sorace, L.; Sessoli, R. Room-temperature quantum coherence and Rabi oscillations in vanadyl phthalocyanine: toward multifunctional molecular spin qubits. *J. Am. Chem. Soc.* **2016**, *138*, 2154–2157.

(19) Yamabayashi, T.; Atzori, M.; Tesi, L.; Cosquer, G.; Santanni, F.; Boulon, M.-E.; Morra, E.; Benci, S.; Torre, R.; Chiesa, M.; Sorace, L.; Sessoli, R.; Yamashita, M. Scaling up electronic spin qubits into a three-dimensional metal–organic framework. *J. Am. Chem. Soc.* **2018**, *140*, 12090–12101.

(20) Ariciu, A.-M.; Woen, D. H.; Huh, D. N.; Nodaraki, L. E.; Kostopoulos, A. K.; Goodwin, C. A. P.; Chilton, N. F.; McInnes, E. J. L.; Winpenny, R. E. P.; Evans, W. J.; Tuna, F. Engineering electronic structure to prolong relaxation times in molecular qubits by minimising orbital angular momentum. *Nat. Commun.* **2019**, *10*, 3330.

(21) Urtizberea, A.; Natividad, E.; Alonso, P. J.; Pérez-Martínez, L.; Andrés, M. A.; Gascón, I.; Gimeno, I.; Luis, F.; Roubeau, O. Vanadyl spin qubit 2D arrays and their integration on superconducting resonators. *Mater. Horiz.* **2020**, *7*, 885–897.

(22) Fataftah, M. S.; Krzyaniak, M. D.; Vlaisavljevich, B.; Wasielewski, M. R.; Zadrozny, J. M.; Freedman, D. E. Metal–ligand covalency enables room temperature molecular qubit candidates. *Chem. Sci.* **2019**, *10*, 6707–6714.

(23) Gaita-Ariño, A.; Luis, F.; Hill, S.; Coronado, E. Molecular spins for quantum computation. *Nat. Chem.* **2019**, *11*, 301–309.

(24) Atzori, M.; Sessoli, R. The second quantum revolution: role and challenges of molecular chemistry. *J. Am. Chem. Soc.* **2019**, *141*, 11339–11352.

(25) Aromí, G.; Roubeau, O. Lanthanide Molecules for Spin-Based Quantum Technologies. In *Handbook on the Physics and Chemistry of Rare Earths*; Elsevier, 2019; Vol. 56, pp 1–54.

(26) Zadrozny, J. M.; Niklas, J.; Poluektov, O. G.; Freedman, D. E. Millisecond coherence time in a tunable molecular electronic spin qubit. *ACS Cent. Sci.* **2015**, *1*, 488–492.

(27) Dai, Y.; Fu, Y.; Shi, Z.; Qin, X.; Mu, S.; Wu, Y.; Su, J.-H.; Deng, Y.-F.; Qin, L.; Zhai, Y.-Q.; Zheng, Y.-Z.; Rong, X.; Du, J. Experimental protection of the spin coherence of a molecular qubit exceeding a millisecond. *Chin. Phys. Lett.* **2021**, *38*, 030303.

(28) Bayliss, S. L.; Laorenza, D. W.; Mintun, P. J.; Kovos, B. D.; Freedman, D. E.; Awschalom, D. D. Optically addressable molecular spins for quantum information processing. *Science* **2020**, *370*, 1309–1312.

(29) Yu, C.-J.; Krzyaniak, M. D.; Fataftah, M. S.; Wasielewski, M. R.; Freedman, D. E. A concentrated array of copper porphyrin candidate qubits. *Chem. Sci.* **2018**, *10*, 1702–1708.

(30) Yu, C.-J.; von Kugelgen, S.; Krzyaniak, M. D.; Ji, W.; Dichtel, W. R.; Wasielewski, M. R.; Freedman, D. E. Spin and phonon design in modular arrays of molecular qubits. *Chem. Mater.* **2020**, *32*, 10200–10206.

(31) Eaton, S. S.; Eaton, G. R. Relaxation Mechanisms. In *EPR Spectroscopy: Fundamentals and Methods*; Goldfarb, D., Stoll, S., Eds.; John Wiley & Sons, 2018; pp 175–192.

(32) Amdur, M. J.; Mullin, K. R.; Waters, M. J.; Puggioni, D.; Wojnar, M. K.; Gu, M.; Sun, L.; Oyala, P. H.; Rondinelli, J. M.; Freedman, D. E. Chemical control of spin–lattice relaxation to discover a room temperature molecular qubit. *Chem. Sci.* **2022**, *13*, 7034–7045.

(33) Dai, Y.-Z.; Dong, B.-W.; Kao, Y.; Wang, Z.-Y.; Un, H.-I.; Liu, Z.; Lin, Z.-J.; Li, L.; Xie, F.-B.; Lu, Y.; Xu, M.-X.; Lei, T.; Sun, Y.-J.; Wang, Y.; Gao, S.; Jiang, S.-D.; Pei, J. Chemical modification toward long spin lifetimes in organic conjugated radicals. *ChemPhysChem* **2018**, *19*, 2972–2977.

(34) Haugland, M. M.; Lovett, J. E.; Anderson, E. A. Advances in the synthesis of nitroxide radicals for use in biomolecule spin labelling. *Chem. Soc. Rev.* **2018**, *47*, 668–680.

(35) Thankamony, A. S. L.; Wittmann, J. J.; Kaushik, M.; Corzilius, B. Dynamic nuclear polarization for sensitivity enhancement in modern solid-state NMR. *Prog. Nucl. Mag. Res. Sp.* **2017**, *102*, 120–195.

(36) Zhang, T.; Pramanik, G.; Zhang, K.; Gulka, M.; Wang, L.; Jing, J.; Xu, F.; Li, Z.; Wei, Q.; Cigler, P.; Chu, Z. Toward quantitative biosensing with nitrogen–vacancy center in diamond. *ACS Sens.* **2021**, *6*, 2077–2107.

(37) Doorslaer, S. V. Hyperfine Spectroscopy – ESEEM. In *EPR Spectroscopy: Fundamentals and Methods*; Goldfarb, D., Stoll, S., Eds.; John Wiley & Sons, 2018; pp 377–400.

(38) Zhou, H.-C.; Long, J. R.; Yaghi, O. M. Introduction to metal–organic frameworks. *Chem. Rev.* **2012**, *112*, 673–674.

(39) Li, H.-Y.; Zhao, S.-N.; Zang, S.-Q.; Li, J. Functional metal–organic frameworks as effective sensors of gases and volatile compounds. *Chem. Soc. Rev.* **2020**, *49*, 6364–6401.

(40) Koo, W.-T.; Jang, J.-S.; Kim, I.-D. Metal–organic Frameworks for chemiresistive sensors. *Chem* **2019**, *5*, 1938–1963.

(41) Marquis, S.; Moissette, A.; Vezin, H.; Brémard, C. Long-lived radical cation−electron pairs generated by anthracene sorption in non Brønsted acidic zeolites. *J. Phys. Chem. B* **2005**, *109*, 3723–3726.

(42) Moissette, A.; Marquis, S.; Cornu, D.; Vezin, H.; Brémard, C. Long-lived spin-correlated pairs generated by photolysis of naphthalene occluded in non-Brønsted acidic ZSM-5 zeolites. *J. Am. Chem. Soc.* **2005**, *127*, 15417–15428.

(43) Kultaeva, A.; Pöppl, A.; Biktagirov, T. Atomic-scale quantum sensing of ensembles of guest molecules in a metal–organic framework with intrinsic electron spin centers. *J. Phys. Chem. Lett.* **2022**, *13*, 6737–6742.

(44) Hmadeh, M.; Lu, Z.; Liu, Z.; Gándara, F.; Furukawa, H.; Wan, S.; Augustyn, V.; Chang, R.; Liao, L.; Zhou, F.; Perre, E.; Ozolins, V.; Suenaga, K.; Duan, X.; Dunn, B.; Yamamto, Y.; Terasaki, O.; Yaghi, O. M. New porous crystals of extended metal–catecholates. *Chem. Mater.* **2012**, *24*, 3511–3513.

(45) Naidek, K. P.; Zuconelli, C. R.; Cruz, O. M.; Ribeiro, R.; Winnischofer, S. M. B.; Winnischofer, H. Characterization of 2,3,6,7,10,11-hexahydroxytriphenylene and its effects on cell viability in human cancer cell lines. *Biochem. Cell Biol.* **2016**, *94*, 205–211.

(46) Misumi, Y.; Yamaguchi, A.; Zhang, Z.; Matsushita, T.; Wada, N.; Tsuchiizu, M.; Awaga, K. Quantum spin liquid state in a two-dimensional semiconductive metal–organic framework. *J. Am. Chem. Soc.* **2020**, *142*, 16513–16517.

(47) Dou, J.-H.; Arguilla, M. Q.; Luo, Y.; Li, J.; Zhang, W.; Sun, L.; Mancuso, J. L.; Yang, L.; Chen, T.; Parent, L. R.; Skorupskii, G.; Libretto, N. J.; Sun, C.; Yang, M. C.; Dip, P. V.; Brignole, E. J.; Miller, J. T.; Kong, J.; Hendon, C. H.; Sun, J.; Dincă, M. Atomically precise single-crystal structures of electrically conducting 2D metal–organic frameworks. *Nat. Mater.* **2021**, *20*, 222–228.

(48) Huang, Z.; Grape, E. S.; Li, J.; Inge, A. K.; Zou, X. 3D electron diffraction as an important technique for structure elucidation of metal–organic frameworks and covalent organic frameworks. *Coord. Chem. Rev.* **2021**, *427*, 213583.

(49) Stoll, S. Pulsed EPR. In *EPR Spectroscopy: Fundamentals and Methods*; Goldfarb, D., Stoll, S., Eds.; John Wiley & Sons, 2018; pp 215–233.

(50) Hu, Y.; Teat, S. J.; Gong, W.; Zhou, Z.; Jin, Y.; Chen, H.; Wu, J.; Cui, Y.; Jiang, T.; Cheng, X.; Zhang, W. Single crystals of mechanically entwined helical covalent polymers. *Nat. Chem.* **2021**, *13*, 660–665.

(51) Tyryshkin, A. M.; Dikanov, S. A.; Goldfarb, D. Sum combination harmonics in four-pulse ESEEM spectra. Study of the ligand geometry in aqua–vanadyl complexes in polycrystalline and glass matrices. *J. Magn. Reason. Ser. A* **1993**, *105*, 271–283.

(52) Milov, A. D.; Samoilova, R. I.; Shubin, A. A.; Grishin, Yu. A.; Dzuba, S. A. ESEEM measurements of local water concentration in D_2O-containing spin-labeled systems. *Appl. Magn. Reason.* **2008**, *35*, 73–94.

(53) Shin, B.; Saxena, S. Substantial contribution of the two im idazole rings of the His13−His14 dyad to Cu(II) binding in amyloid-β(1−16) at physiological pH and its significance. *J. Phys. Chem. A* **2011**, *115*, 9590–9602.

(54) Langmuir, I. The adsorption of gases on plane surfaces of glass, mica and platinum. *J. Am. Chem. Soc.* **1918**, *40*, 1361–1403.

(55) Rudd, N. D.; Liu, Y.; Tan, K.; Chen, F.; Chabal, Y. J.; Li, J. Luminescent metal–organic framework for lithium harvesting applications. *ACS Sustainable Chem. Eng.* **2019**, *7*, 6561–6568.

(56) Kamenica, M.; Kothur, R. R.; Willows, A.; Patel, B. A.; Cragg, P. J. Lithium ion sensors. *Sensors* **2017**, *17*, 2430.

(57) Mitrikas, G.; Prokopiou, G. Modulation depth enhancement of ESEEM experiments using pulse trains. *J Magn. Reason.* **2015**, *254*, 75–85.

(58) Ellison, W. J. Permittivity of pure water, at standard atmospheric pressure, over the frequency range 0–25 THz and the temperature range 0–100 °C. *J. Phys. Chem. Ref. Data* **2007**, *36*, 1–18.

(59) Zhang, X.; Wolf, C.; Wang, Y.; Aubin, H.; Bilgeri, T.; Willke, P.; Heinrich, A. J.; Choi, T. Electron spin resonance of single iron phthalocyanine molecules and role of their non-localized spins in magnetic interactions. *Nat. Chem.* **2022**, *14*, 59–65.

Room-Temperature Quantitative Quantum Sensing of Li^+